applied sciences

MDPI

Article

Low-Complexity Hybrid Optical OFDM with High Spectrum Efficiency for Dimming Compatible VLC System

Simeng Feng [1], Hailiang Feng [2], Ying Zhou [3] and Baolong Li [3,*]

[1] Next Generation Wireless, University of Southampton, Southampton SO17 1BJ, UK
[2] Academy of Broadcasting Science, National Radio and Television Administration, Beijing 100866, China
[3] Jiangsu Provincial Engineering Laboratory of Pattern Recognition and Computational Intelligence, Jiangnan University, Wuxi 214122, China
* Correspondence: lblong@jiangnan.edu.cn; Tel.: +86-134-5181-4793

Received: 31 July 2019; Accepted: 2 September 2019; Published: 4 September 2019

Abstract: In visible light communications (VLC), dimming control constitutes an indispensable technique to comply with various illumination necessities and with different energy consumption constraints. Therefore, a novel dimming compatible hybrid optical orthogonal frequency division multiplexing (DCHO-OFDM) is conceived in this paper to fulfil the requirements from communications and illuminations. Explicitly, the signal branch of the unclipped asymmetrically clipped O-OFDM (ACO-OFDM) and the down/upper-clipped pulse-amplitude-modulated discrete multitone (PAM-DMT) are adaptively amalgamated in order to increase the spectrum efficiency. For the sake of precisely achieving dimming control, the chromaticity-shift-free and industry-preferred pulse width modulation (PWM) is further invoked to the hybrid signal, assisted by a time-varying biasing scheme to mitigate the non-linear distortion. As the different signal components in DCHO-OFDM are beneficially combined in an interference-orthogonal approach, the transmitted symbols are able to be readily detected upon relying on a standard OFDM receiver, as that of ACO-OFDM. Our simulations demonstrate that a high spectrum efficiency of the conceived DCHO-OFDM scheme can be achieved with less fluctuation in a wide dimming range.

Keywords: visible light communications (VLC); optical orthogonal frequency division multiplexing (O-OFDM); dimming control; pulse width modulation (PWM)

1. Introduction

Driven by the rapid development of light emitting diodes (LED), visible light communication (VLC) constitutes a promising part of next-generation wireless communications [1–3]. Under the trend of internet of everything (IoE), the exhaustion of radio frequency (RF) band to resolve the unprecedented data escalation dilemma becomes a bottleneck of current communications [4,5]. As a benefit, the environmentally friendly technology of VLC possesses plenty of unlicensed spectral resource at the high frequency band [6]. This part of electromagnetic-interference-free spectrum can be exploited, for the sake of supporting high-speed and high-security communications in the near future [7]. Upon relying on modulating the intensity of lights above the flicker-fusion frequency, the dual functionality of communications and illuminations can be simultaneously achieved in VLC, providing an efficient solution especially for short-range communications [8].

In order to achieve high-speed transmission, optical orthogonal frequency division multiplexing (O-OFDM) modulation schemes have been extensively explored for VLC systems [9]. Since a VLC system is based on intensity modulation and direct detection (IM/DD), the transmitted signal via

VLC link should be both real-valued and positive-valued [10]. To meet these constraints, there are two classic O-OFDM schemes in VLC, namely, asymmetrically clipped O-OFDM (ACO-OFDM) and DC-biased O-OFDM (DCO-OFDM). DCO-OFDM relies on a DC bias to guarantee the positivity, which enjoys the advantage of implementation simplicity. However, it suffers from the power inefficiency since the DC bias which does not convey any information leads to a waste of power. By contrast, with the aid of the properties of Fourier transform, ACO-OFDM directly clips the negative parts of the signal to generate a non-negative signal, substantially increasing the power efficiency, but ACO-OFDM leverages only half of the subcarriers for transmission hence, resulting in spectrum inefficiency [11]. Therefore, advanced transmission schemes have been further investigated, such as hybrid ACO-OFDM (HACO-OFDM) [12] and layered ACO-OFDM (LACO-OFDM) [13]. In HACO-OFDM regimes, for the sake of promoting the spectrum efficiency, the ACO-OFDM signal is further combined with pulse-amplitude-modulated discrete multitone (PAM-DMT), where the latter is employed to modulate the imaginary part of even-indexed subcarriers. Superior to the conventional OFDM schemes, HACO-OFDM can notably improve the spectrum efficiency while, at the same time, maintaining high power efficiency. However, on the receiver side of HACO-OFDM, additional operations including the re-generation of time-domain ACO-OFDM samples, the zero-clipping, the re-production of clipping distortion and the noise subtraction are required, leading to an increased complexity [14]. The perspective of LACO-OFDM improves the traditional ACO-OFDM upon relying on actively invoking the unexploited subcarriers for transmission in a layer-based approach. Compared to HACO-OFDM, the spectrum efficiency can be further enhanced. Unfortunately, the improvement of spectrum efficiency in LACO-OFDM is accompanied by the complexity increment due to the multi-layer transmitter and the successive interference cancellation (SIC) receiver [15].

It is worth mentioning that conventional O-OFDM schemes mainly concentrate on promoting data rate, while ignoring the various illumination requirements. As an emerging member of green communication technology, VLC is intrinsically distinct from the conventional RF system due to its dual functionality: communications and ambient lighting, and not just the former [16]. Therefore, the dimming control is envisioned to be a critical technique in VLC, for the sake of handling the lighting and energy consumption constraints [17]. There are mainly two kinds of dimming approaches extensively used in VLC, namely, analogous dimming and digital dimming. A popular analogous dimming approach, known as the conventional DCO-OFDM, achieves dimming control upon adjusting the DC bias, which is easily implemented. Unfortunately, the performance of DCO-OFDM may fluctuate with different dimming levels. Especially when the requested dimming level is considerably low or high, the resulting performance becomes degraded, due to the grave non-linear distortion [18]. The analogous dimming approach is further investigated in terms of advanced O-OFDM scheme, such as the asymmetrical hybrid optical-OFDM (AHO-OFDM) scheme [19]. In AHO-OFDM, either the signal of PAM-DMT or ACO-OFDM is inverted, and then compounded for transmission. By modifying the power allocated to the two components, a wide dimming range can be attained. However, the analogous dimming approach is challenging to precisely control the brightness and may further impinge upon the wavelength of the emitted light, resulting in undesired chromaticity shift [20]. Therefore, another category of the dimming approach, which is referred to as digital dimming relying on the the pulse width modulation (PWM) technique has been extensively applied. A reverse polarity O-OFDM (RPO-OFDM) was proposed to dim the transmitted signal, such as the conventional ACO-OFDM, upon invoking the PWM technique [21]. RPO-OFDM can realize a steady BER performance over a wide range of dimming levels, but has a low spectrum efficiency. To improve the spectrum efficiency, a negative HACO-OFDM (NHACO-OFDM) scheme was conceived in [22] for combining with the high level of PWM signal, which is further amalgamated with HACO-OFDM at the low level. In this regime, the various dimming requests can be satisfied upon altering the proportion of these two branches, while a high spectral efficiency can be realized. Moreover, the authors in [23] proposed a reconstructed layered ACO-OFDM (RLACO-OFDM) scheme based on LACO-OFDM, which is further combined with PWM signal to achieve various brightness levels, without introducing additional complexity. As a benefit, the PWM-biased dimming approach constitutes an implementation-friendly philosophy, where the brightness level can be well-controlled upon varying the parameter of duty cycle [24].

However, the existing digital dimming approaches are vulnerable to the varying dimming level, where a preliminary is required at the receiver side to detect the PWM signal, leading to an increasing complexity. In fact, detecting the PWM signal may be intractable especially in the scenario of multiple LEDs, since the received multi-path signals may have different dimming levels [23]. Furthermore, as mentioned above, both the HACO-OFDM and LACO-OFDM require a successive demodulation operation, suffering from an increased receiver complexity. Against this background, *a novel dimming compatible hybrid optical OFDM (DCHO-OFDM) is conceived in this paper incorporating the PWM technique to realize high-spectral-efficiency transmission under various dimming levels, where the transmitted signal can be readily recovered upon relying on a standard receiver.* To be specific,

- The conceived DCHO-OFDM signal is beneficially composed of the unclipped ACO-OFDM signal and the down/upper-clipped unipolar PAM-DMT signal, where the time-varying bias is further facilitated to diminish the undesired non-linear distortion. In this way, the proposed DCHO-OFDM achieves a higher spectrum efficiency than the conventional schemes over a broad dimming range.
- Thanks to the elaborately combined signal, the symbol transmitted by the proposed DCHO-OFDM is capable of being recovered without detecting the PWM signal, which is superior to the existing digital dimming approaches. Additionally, the BER performance of DCHO-OFDM is invulnerable to the various duty cycles of PWM, achieving a steady system performance in a wide dimming range compared to DCO-OFDM.
- Moreover, the information-carried subcarriers in the proposed DCHO-OFDM scheme can avoid the corruption by the generated interference. As a benefit, the symbols transmitted by the proposed DCHO-OFDM can be readily detected upon relying on a standard OFDM receiver, which significantly reduces the complexity at receiver compared to the existing advanced transmission schemes, such as HACO-OFDM and LACO-OFDM.

The superiorities of the proposed DCHO-OFDM in terms of spectrum efficiency over its counterparts have been verified by our simulation results.

The rest of this paper is organized as follows. Section 2 provides a review of the HACO-OFDM scheme in VLC. The detail of the proposed DCHO-OFDM regime is presented in Section 3. Our numerical results are discussed in Section 4, whilst our conclusions are drawn in Section 5.

2. Brief Review of HACO-OFDM

To enhance the spectrum efficiency, HACO-OFDM scheme amalgamates the signal of ACO-OFDM with PAM-DMT for achieving an ambitious transmission rate [12]. In order to guarantee real-valued outputs, Hermitian symmetry is invoked in each branch. As demonstrated in Figure 1a, the mapped M-ary quadrature amplitude modulation (M-QAM) symbols A_i in ACO-OFDM branch occupy the odd-indexed subcarriers, which is expressed as:

$$\mathbf{X} = \left[0, A_1, 0, A_2, \cdots, A_{N/4}, 0, A^*_{N/4}, \cdots, A^*_2, 0, A^*_1\right], \tag{1}$$

where the total number of subcarriers is denoted by N and A^*_i is invoked to present the Hermitian symmetry of symbol A_i. After performing the N-point IFFT of $\mathbf{X}$, a bipolar time-domain signal $x_{ACO,n}$ is obtained. In order to acquire the positive signal appropriating for VLC propagation, the bipolar signal of $x_{ACO,n}$ has to be directly clipped at zero as:

$$\lfloor x_{ACO,n} \rfloor_c = \begin{cases} 0, & x_{ACO,n} < 0 \\ x_{ACO,n}, & x_{ACO,n} \geq 0 \end{cases}, \tag{2}$$

where the resultant clipping distortion is imposed on the even-indexed subcarriers, leaving the odd-indexed subcarriers carrying ACO-OFDM symbols uncontaminated [25]. For the PAM-DMT link, as depicted in Figure 1a, the mapped L-ary pulse amplitude modulation (L-PAM) symbols B_i are assigned to the the even-indexed subcarriers, with only the imaginary component being modulated. It can be expressed as:

$$\mathbf{Y} = \left[0, 0, jB_1, 0, jB_2, \cdots, jB_{N/4-1}, 0, 0, 0, jB^*_{N/4-1}, 0, \cdots, jB^*_2, 0, jB^*_1, 0\right], \tag{3}$$

where we have $j = \sqrt{-1}$. A bipolar signal of $y_{PAM,n}$ can be then obtained, upon performing the N-point IFFT operation of $\mathbf{Y}$. For the sake of producing the non-negative result, $y_{PAM,n}$ is clipped at zero-level, which is given by:

$$\lfloor y_{PAM,n} \rfloor_c = \begin{cases} 0, & y_{PAM,n} < 0 \\ y_{PAM,n}, & y_{PAM,n} \geq 0 \end{cases}. \tag{4}$$

Consequently, in HACO-OFDM scheme, the clipped signal $\lfloor x_{ACO,n} \rfloor_c$ and $\lfloor y_{PAM,n} \rfloor_c$ is capable of being simultaneously transmitted, achieving a beneficially high spectrum efficiency. As the detrimental clipping noise generated by ACO-OFDM contaminates the subcarriers carrying PAM-DMT signal, the receiver of HACO-OFDM has to recover the ACO-OFDM symbols first and then retrieve the clipping distortion imposed on the even-indexed subcarriers, so that the detection of PAM-DMT signal can be successively implemented.

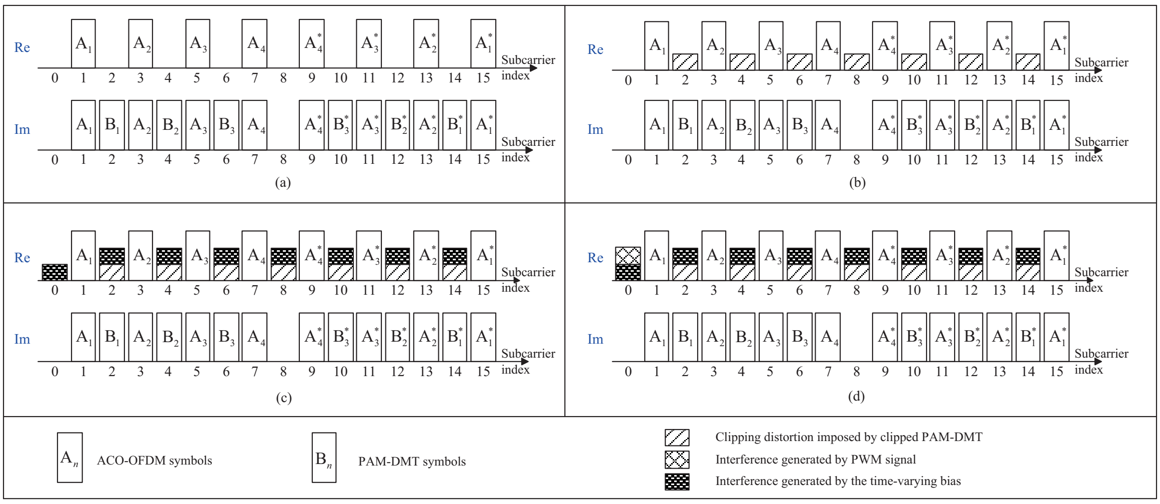

Figure 1. Frequency-domain demonstration including both the real component and the imaginary component of the proposed DCHO-OFDM signal, with $N = 16$ subcarriers. (**a**) presents the symbol allocation for ACO-OFDM and for PAM-DMT branch, respectively; (**b**) demonstrates the hybrid unclipped ACO-OFDM and the down/upper-clipped PAM-DMT signals; (**c**) indicates the combined signal after performing time-varying biasing scheme; (**d**) depicts the hybrid signal further incorporating the PWM signal.

For achieving dimming control, directly combining the HACO-OFDM signal with PWM is deemed to be inefficient. Due to the non-negativity of the clipped unipolar signal $\lfloor x_{ACO,n} \rfloor_c$ and $\lfloor y_{PAM,n} \rfloor_c$, the hybrid signal may exceed the dynamic range of LEDs with a large probability [26]. To overcome, a negative-valued NHACO-OFDM signal is invoked to superpose to the high brightness level of PWM signal to avoid non-linear distortion, while the HACO-OFDM with positive-polarity is invoked for the low-brightness scenario [22]. In this regime, the PWM signal has to be detected first by a receiver in order to recover the dissimilar clipping distortion generated by NHACO-OFDM and HACO-OFDM, respectively. Afterwards, the transmitted information can be then extracted by successively demodulating the ACO-OFDM and PAM-DMT branch.

3. Proposed Dimming Compatible Hybrid O-OFDM

Although the spectrum efficiency is improved in HACO-OFDM, the sequential detection operations lead to an increased receiver complexity and process delay, compared to that of the conventional ACO/DCO-OFDM. When dimming control is invoked, additional operation including the detection of PWM signal is necessary before demodulation, which further increases the implementation complexity. To overcome this, in this paper, a novel dimming compatible hybrid O-OFDM (DCHO-OFDM) scheme is conceived with a low-complexity receiver for achieving a high-speed VLC transmission. Moreover, the proposed scheme is insensitive to the different dimming levels, which implies the preliminary of detecting PWM signal can be neglected.

3.1. Pulse Width Modulation

Due to the non-linear transfer characteristic of LED, the transmitted VLC signal has to be confined in the limited linear range. We employ the notation I_l and I_h to represent the lower and upper bound of the limited linear range, respectively. Then, the dimming level η can be defined as:

$$\eta = \frac{I_{ave} - I_l}{I_h - I_l}, \tag{5}$$

where we have I_{ave} to present the average amplitude of signal. Upon observing Equation (5), different dimming levels can be attained by altering the value of I_{ave}. Although directly adding a bias can change the value of I_{ave}, it leads to an undesired wavelength shift of the emitted lights. Therefore, the PWM signal is invoked in our proposed DCHO-OFDM scheme, which can be expressed as:

$$d_{PWM}(t) = \begin{cases} I_h, & 0 < t \leq T_{ON} \text{ (ON state)} \\ I_l, & T_{ON} < t \leq T \text{ (OFF state)} \end{cases} \tag{6}$$

where T represents the period of PWM signal and T_{ON} denotes the time duration when the signal is in the ON state. The dimming level can be changed upon adjusting the duty cycle of PWM, which is referred to as $\rho = T_{ON}/T$.

3.2. DCHO-OFDM

In order to implement dimming control, the PWM signal needs to be designated for incorporating the O-OFDM transmission. Specifically, the period of the PWM is set to be as many as the K times of a single O-OFDM symbol duration T_s, which can be represented as $T = KT_s$, where K is an integer. Accordingly, the duration of ON state of PWM is set to $T_{ON} = K'T_s$, where K' denotes the number of O-OFDM symbols transmitted at ON state. It can be observed that the PWM signal remains constant in a single O-OFDM symbol duration T_s, which implies that the introduced interference is imposed only on the 0-th subcarrier, as depicted in Figure 1d.

Since the transmitted signal in VLC has to be constrained by the limited linear transmission range of LEDs, the O-OFDM components needs to be carefully designed, in order to incorporate PWM for the purpose of dimming control. Taking the characteristic of the PWM signal into consideration, a signal with negative polarity is desired during the ON state, while a positive-valued signal is required for the OFF state. Therefore, instead of combining the unipolar signal of ACO-OFDM and of PAM-DMT as seen in the conventional HACO-OFDM scheme, we invoke the unclipped double-side ACO-OFDM signal in our proposed DCHO-OFDM to amalgamated with either the upper-clipped PAM-DMT signal $\lceil y_{PAM,n} \rceil_c$ or the down-clipped PAM-DMT signal $\lfloor y_{PAM,n} \rfloor_c$ as:

$$\begin{cases} s_n^{on} = x_{ACO,n} + \lceil y_{PAM,n} \rceil_c, & \text{ON state} \\ s_n^{off} = x_{ACO,n} + \lfloor y_{PAM,n} \rfloor_c, & \text{OFF state} \end{cases}, \tag{7}$$

depending on the state of PWM signal. Note that the upper-clipped PAM-DMT signal is given by:

$$\lceil y_{PAM,n} \rceil_c = \begin{cases} 0, & y_{PAM,n} \geq 0 \\ y_{PAM,n}, & y_{PAM,n} < 0 \end{cases}. \tag{8}$$

Similar to the HACO-OFDM scheme, the ACO-OFDM symbols in our DCHO-OFDM are allocated to the odd-indexed subcarriers, where the PAM-DMT symbols are carried by the imaginary proportion of the even-indexed subcarriers, as shown in (1) and (3). On the contrary, the ACO-OFDM branch in the proposed DCHO-OFDM scheme is designed to remain unclipped, yielding even-indexed subcarriers that are free of clipping noise contamination. According to [27], the clipping distortion generated by the down-clipped PAM-DMT is imposed only on the real-part of the even-indexed subcarriers. Furthermore, upon the analysis provided in Appendix A, the clipping distortion caused by the upper-clipped PAM-DMT is also encountered only by the real-portion of the even-indexed subcarriers. Therefore, it implies that the overall generated clipping distortion in DCHO-OFDM of either the combined signal s_n^{on} or s_n^{off} is orthogonal to the information-carrying subcarriers, which is demonstrated in Figure 1b. As a benefit, the bipolar signal of s_n^{on} and s_n^{off} can be obtained in an interference-orthogonal way. Furthermore, in HACO-OFDM scheme, the clipped ACO-OFDM and PAM-DMT branch are superposed directly, which leads to a higher amplitude since the both components are non-negative. In contrast, by superposing the bipolar ACO-OFDM and the unipolar PAM-DMT signal, a lower peak-to-average-power-ratio (PAPR) can be expected, compared to that of the conventional HACO-OFDM.

The hybrid signal in Equation (7) has double-sided polarity, as seen in Figure 2a,b. In order to incorporate the PWM signal, it has to be converted to the unipolar signal. To tackle this issue, we introduce a time-varying biasing scheme based on the Proposition 1, which converts the the bipolar signal of s_n^{on} and s_n^{off} to negative-valued and positive-valued signals for the ON and OFF states, respectively. Moreover, the time-varying bias does not induce any additional interference imposed on the legitimate transmitted symbols. To be specific, the Proposition 1 is exhibited as follows.

Proposition 1. *If a time-domain signal z_n has the characteristic as:*

$$\begin{cases} z_n = z_{\frac{N}{2}+n}, & n = 0, \frac{N}{4} \\ z_n = z_{\frac{N}{2}-n} = z_{\frac{N}{2}+n} = z_{N-n}, & n = 1, \cdots, \frac{N}{4} - 1 \end{cases}, \tag{9}$$

the interference generated by z_n imposes only on the real-part of the even-indexed subcarriers.

Proof. Please see Appendix B. □

For the hybrid signal s_n^{on}, it is expected to be negative for further incorporating the PWM signal during ON state. In the light of Proposition 1, a bias of $-\max\left\{s_n^{on}, s_{N/2+n}^{on}\right\}$ can be added to sample s_n^{on} and $s_{N/2+n}^{on}$, for $n = 0, N/4$, so that to achieve the negative-valued samples. Uniformly, a bias of $-\max\left\{s_n^{on}, s_{N/2-n}^{on}, s_{N/2+n}^{on}, s_{N-n}^{on}\right\}$ is applied for sample $s_n^{on}, s_{N/2-n}^{on}, s_{N/2+n}^{on}$, and s_{N-n}^{on} to acquire the non-positive values, when we have $n = 1, 2, \cdots, N/4 - 1$. Therefore, the introduced time-varying bias z_n^{on} for signal s_n^{on} is given by:

$$\begin{cases} z_n^{\text{on}} = z_{\frac{N}{2}+n}^{\text{on}} = -\max\left\{ s_n^{\text{on}},\ s_{\frac{N}{2}+n}^{\text{on}} \right\}, & n = 0, \frac{N}{4} \\ z_n^{\text{on}} = z_{\frac{N}{2}-n}^{\text{on}} = z_{\frac{N}{2}+n}^{\text{on}} = z_{N-n}^{\text{on}} & \\ \quad = -\max\left\{ s_n^{\text{on}}, s_{\frac{N}{2}-n}^{\text{on}}, s_{\frac{N}{2}+n}^{\text{on}}, s_{N-n}^{\text{on}} \right\}, & n = 1, \cdots, \frac{N}{4}-1 \end{cases}. \tag{10}$$

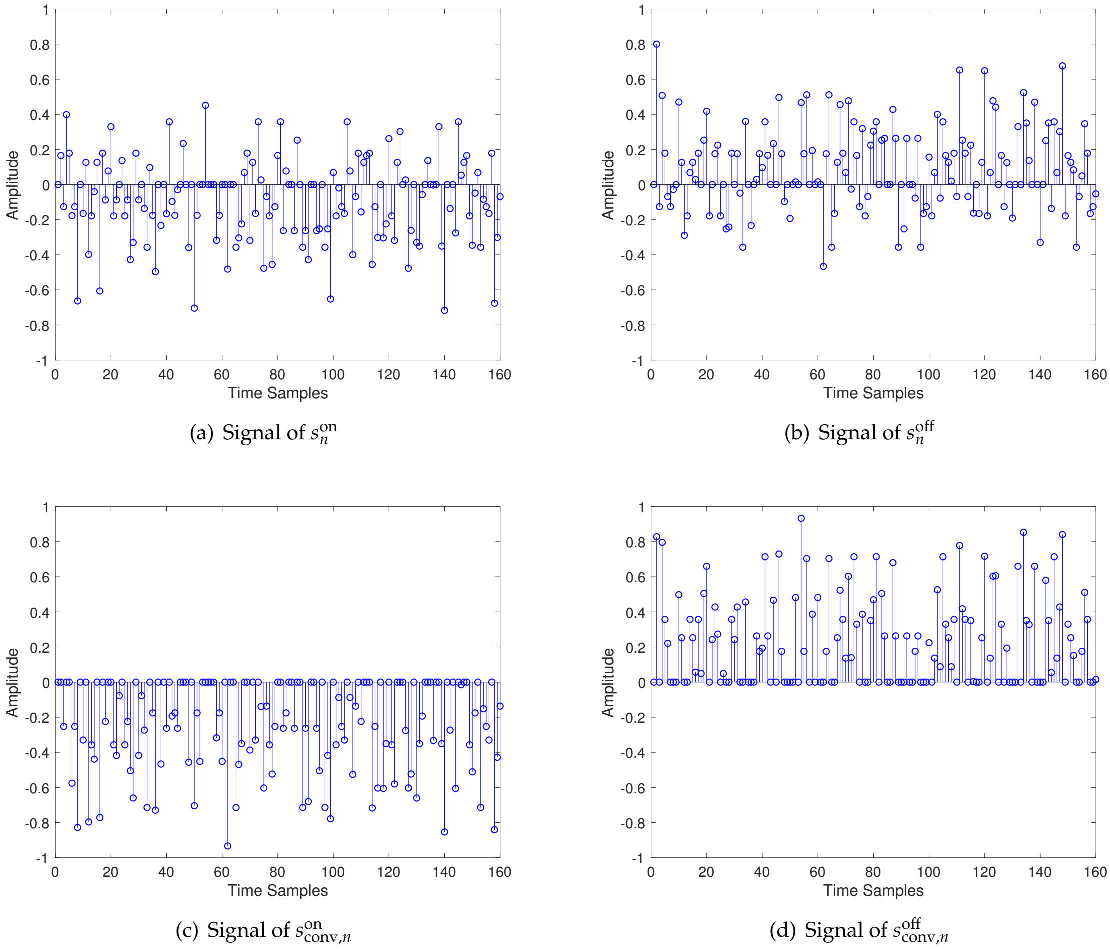

Figure 2. A demonstration of the superposed signal in DCHO-OFDM. (**a**,**b**) depict the bipolar signal s_n^{on} and s_n^{off}, where the ACO-OFDM signal is directly combined with upper/down-clipped PAM-DMT; (**c**,**d**) present the unipolar signal of $s_{\text{conv},n}^{\text{on}}$ and $s_{\text{conv},n}^{\text{off}}$, aided by the introduced time-varying biasing scheme.

After performing the time-varying biasing, the bipolar signal s_n^{on} is able to be converted to the unipolar signal as:

$$s_{\text{conv},n}^{\text{on}} = x_{ACO,n} + \lceil y_{PAM,n} \rceil_c + z_n^{\text{on}}, \quad n = 0, 1, \cdots, N-1, \tag{11}$$

where all the N samples experience non-positive values, which is demonstrated in Figure 2c. On the contrary, a positive-valued signal is desired during OFF state transmission. Therefore, for the bipolar signal s_n^{off}, the time-varying bias z_n^{off} is introduced as:

$$\begin{cases} z_n^{\text{off}} = z_{\frac{N}{2}+n}^{\text{off}} = -\min\left\{s_n^{\text{off}}, s_{\frac{N}{2}+n}^{\text{off}}\right\}, & n = 0, \frac{N}{4} \\ z_n^{\text{off}} = z_{\frac{N}{2}-n}^{\text{off}} = z_{\frac{N}{2}+n}^{\text{off}} = z_{N-n}^{\text{off}} & \\ \quad = -\min\left\{s_n^{\text{off}}, s_{\frac{N}{2}-n}^{\text{off}}, s_{\frac{N}{2}+n}^{\text{off}}, s_{N-n}^{\text{off}}\right\}, & n = 1, \cdots, \frac{N}{4}-1 \end{cases}. \tag{12}$$

Hence, the converted signal is given by:

$$s_{\text{conv},n}^{\text{off}} = x_{ACO,n} + \lfloor y_{PAM,n} \rfloor_c + z_n^{\text{off}}, \quad n = 0, 1, \cdots N-1, \tag{13}$$

resulting in a positive-valued signal as shown in Figure 2d, which is appropriated for OFF state transmission.

Assisted by the time-varying biasing scheme, the acquired unipolar signals relying on the Equations (11) and (13) can be readily amalgamated with PWM signal. To this end, the proposed DCHO-OFDM signal can be expressed as:

$$\begin{aligned} v_n &= \begin{cases} s_{\text{conv},n}^{\text{on}} + I_h, & \text{ON state} \\ s_{\text{conv},n}^{\text{off}} + I_l, & \text{OFF state} \end{cases} \\ &= s_{\text{conv},n} + d_{PAM,n}, \quad n = 0, 1, \cdots, N-1. \end{aligned} \tag{14}$$

Note that the signal of $s_{\text{conv},n}$ consists of the ON state transmitted signal, $s_{\text{conv},n}^{\text{on}}$, and the OFF state transmitted signal, $s_{\text{conv},n}^{\text{off}}$, while $d_{PAM,n}$ is the sample of PWM signal $d_{PAM}(t)$. It is observed from Equation (14) that the PWM dimming control and the OFDM transmission can be well integrated in the conceived DCHO-OFDM. Specifically, Figure 3 depicts the block diagram of the proposed DCHO-OFDM.

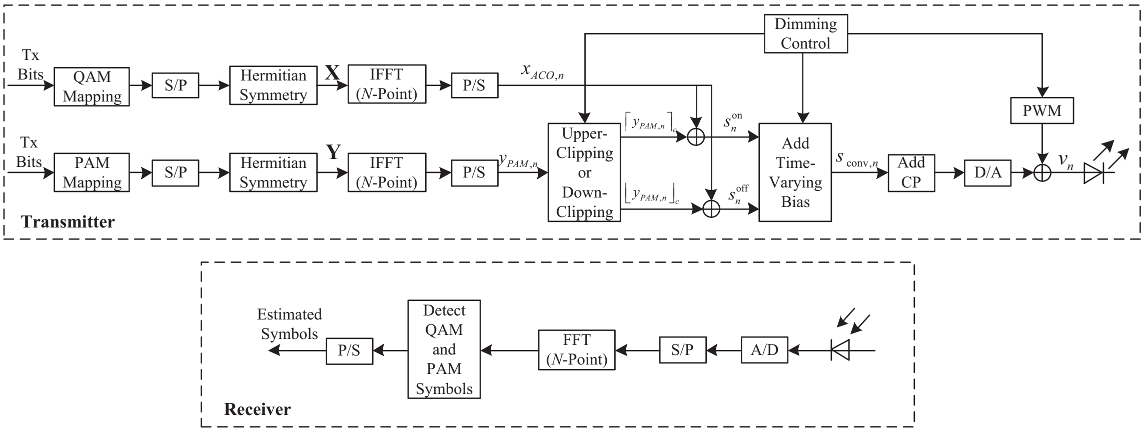

Figure 3. Block diagram of the transmitter and receiver for the proposed DCHO-OFDM.

Furthermore, according to Equation (14), the average amplitude of signal v_n is given by:

$$\begin{aligned} I_{ave} &= \frac{T_{ON}}{T}\left(I_h + \mathbb{E}\left[s_{\text{conv},n}^{\text{on}}\right]\right) + \frac{T - T_{ON}}{T}\left(I_l + \mathbb{E}\left[s_{\text{conv},n}^{\text{off}}\right]\right) \\ &= I_l + E_1 + \rho(I_h - I_l + E_2 - E_1) \end{aligned} \tag{15}$$

where $\mathbb{E}[\bullet]$ denoted the expectation operation. Here, we have E_1 and E_2 to denote the expectation result of signal $s_{\text{conv},n}^{\text{off}}$ and $s_{\text{conv},n}^{\text{on}}$, respectively, which can be readily obtained by numerical simulations. Recalling the Equation (5), the dimming level can then be further expressed as:

$$\eta = \frac{E_1}{I_h - I_l} + \rho\left[1 + \frac{E_2 - E_1}{I_h - I_l}\right]. \tag{16}$$

The Equation (16) shows that the dimming level η has a linear relationship with the duty cycle ρ.

It is essential to discuss the receiver structure for the proposed DCHO-OFDM scheme. The clipping distortion caused by down/upper-clipped PAM-DMT branch in DCHO-OFDM is orthogonal to the information-carrying subcarriers. Moreover, in the light of Proposition 1, the odd-indexed subcarriers carrying ACO-OFDM and the imaginary-part of the even-indexed subcarriers carrying PAM-DMT is capable of remaining uncontaminated during the polarity conversion process relying on the introduced time-varying bias, which is demonstrated in Figure 1c. When the converted signal is amalgamated with PWM for dimming control, the interference caused by PWM falls only on the 0-th subcarrier, which does not introduce additional interference to the transmitted signal. As a benefit, the DCHO-OFDM signal is obtained in an interference-orthogonal approach. Therefore, DCHO-OFDM symbols can be readily recovered upon relying on a standard OFDM receiver, as shown in Figure 3.

3.3. Complexity Analysis

In this section, the complexity of the proposed DCHO-OFDM is discussed. For comparison, the conventional HACO-OFDM is invoked as a benchmarker. At the transmitter side, the main difference between the conventional HACO-OFDM and the proposed scheme lies in the signal component. To elaborate, the zero-clipping operation of the ACO-OFDM branch is required in HACO-OFDM, while the time-varying biasing process is introduced in the proposed DCHO-OFDM. Remarkably, the zero-clipping operation of ACO-OFDM branch is based on computing the maximum value between zero and the signal sample, which is similar to the calculation process of the time-varying biasing scheme in the proposed DCHO-OFDM. Therefore, the proposed DCHO-OFDM is capable of achieving the similar complexity as the conventional HACO-OFDM at the transmitter.

At the receiver side, due to the undesired clipping distortion generated by the ACO-OFDM branch, an additional process including the clipping noise re-generation and cancellation is required in HACO-OFDM. Therefore, the associated computational complexity mainly relies on the sum of two real-valued N-point FFT operations and of one complex-valued N-point IFFT operation [14]. On the contrary, a benefit to the orthogonal interference, the detection of DCHO-OFDM, can be achieved upon relying on a standard OFDM receiver seen in Figure 3, as that of ACO/DCO-OFDM. Hence, the computational complexity of DCHO-OFDM is dominated by a single real-valued N-point FFT operation, which is significantly reduced compared to the HACO-OFDM counterpart [28]. Moreover, for the HACO-OFDM-based dimming control scheme [22], an additional operation is required at the receiver side to distinguish if either HACO-OFDM or NHACO-OFDM is transmitted, since they introduce different clipping distortions. Instead, the proposed DCHO-OFDM signal is invulnerable to the varying dimming level and can be directly recovered without detecting the PWM signal, which futher reduces the complexity compared to that of the HACO-OFDM scheme.

To this end, superior to the conventional HACO-OFDM scheme, the complexity and the process delay of the proposed DCHO-OFDM scheme at the receiver is significantly reduced, without increasing the complexity at the transmitter side.

4. Numerical Results

This section provides our simulations for quantifying the proposed DCHO-OFDM, where we employ $N = 256$ for the O-OFDM VLC system. The lower bound and the upper bound of LED are referred to as $I_l = 0$ and $I_h = 1$, respectively. In order to evaluate the non-linear distortion, a pair of scaling factors β_{ACO} and β_{PAM} are defined as $\beta_{ACO} = (I_h - I_l)/\sigma_{ACO}$ and $\beta_{PAM} = (I_h - I_l)/\sigma_{PAM}$, where σ_{ACO} and σ_{PAM} denote the standard variance of the unclipped ACO-OFDM and PAM-DMT, respectively.

To begin with, we investigate the PAPR performance of the proposed DCHO-OFDM scheme, compared to that of the HACO-OFDM, where the associated complimentary cumulative distribution function (CCDF) can be seen in Figure 4 [26]. It is observed that the proposed DCHO-OFDM achieves a much lower PAPR than that of the conventional HACO-OFDM. This observation is as expected for the reason that the unclipped ACO-OFDM is invoked in DCHO-OFDM, which is capable of avoiding relatively high amplitudes. Note that a lower PAPR results in a better ability to resist the non-linearity [26]. Therefore, unlike the HACO-OFDM, the proposed OFDM scheme is capable of alleviating the undesired non-linear distortion in the presence of the non-linear transfer characteristic of LED. In this case, a better BER performance can be achieved by the proposed DCHO-OFDM, leading to an improved achievable spectrum efficiency compared to HACO-OFDM, as shown in the following figures.

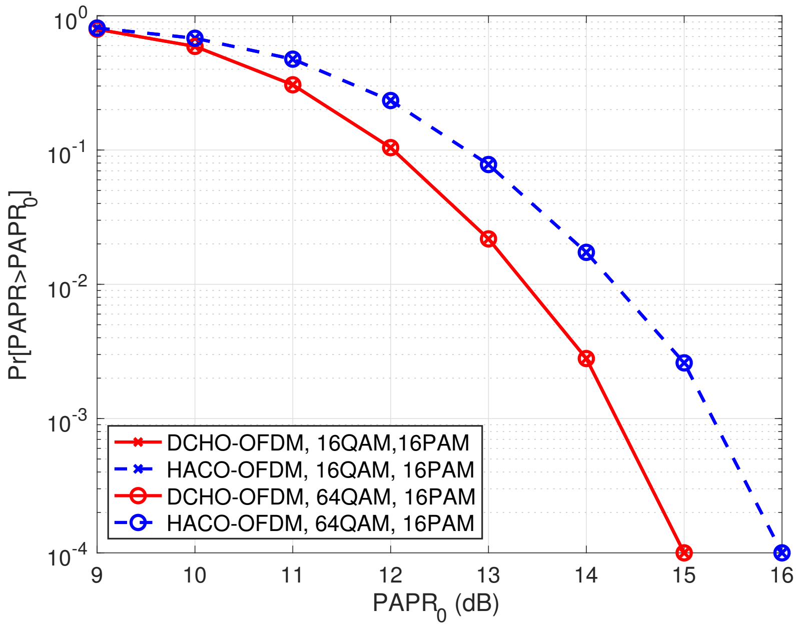

Figure 4. CCDF curves of PAPR for the proposed DCHO-OFDM scheme, compared to that of the HACO-OFDM scheme.

Figure 5 quantifies the dimming level for the various values of duty cycle ρ. Upon observing, the dimming level is linearly changed upon adjusting the duty cycle of PWM signal, which is consistent with our theoretical analysis in Section 3.2. Additionally, a wide range of dimming level is achieved in DCHO-OFDM. To expound, the proposed scheme is capable of achieving a fairly low or high dimming level, upon further increasing the value of the scaling factors, albeit at a cost to power inefficiency.

In Figure 6, we demonstrate the BER performance of DCHO-OFDM vs the variance of signal under different values of duty cycle, where a standard OFDM receiver is directly employed. Upon observing Figure 6, the attained BER of the proposed scheme first becomes better upon increasing the variance of signal, while it deteriorates afterwards due to the clipping noise generated by the limited dynamic range of LEDs. Additionally, we observe that the same BER performance is obtained with various values of duty cycle ρ, which indicates that the BER performance of DCHO-OFDM is invulnerable to the various duty cycles of PWM. This can be explained by noting that the dimming control in the proposed DCHO-OFDM scheme does not affect the information transmission, so that both the functionality of illuminations and communications in VLC can be achieved without disturbing each other. Hence, the symbols transmitted by the proposed DCHO-OFDM can be directly detected through a standard OFDM receiver without requiring additional operation of PWM signal detection.

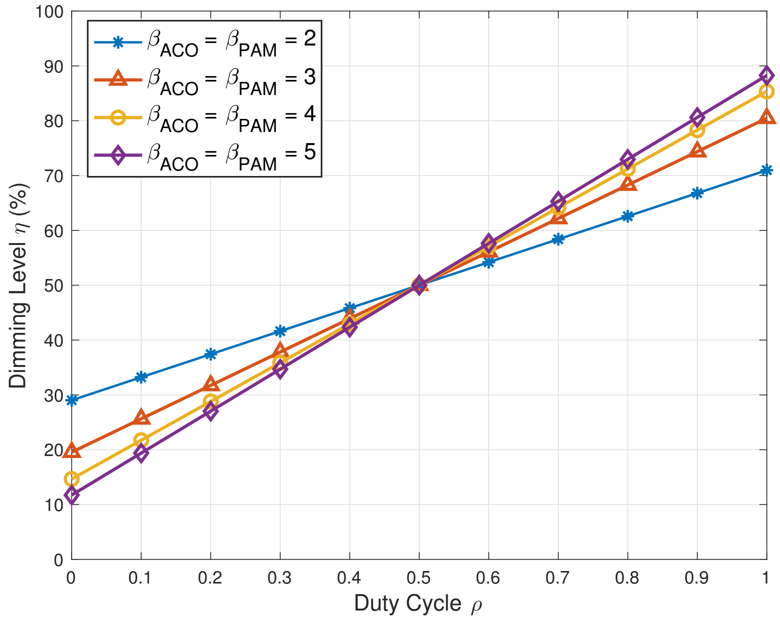

Figure 5. The performance of dimming level η vs duty cycle ρ, with various values of scaling factors.

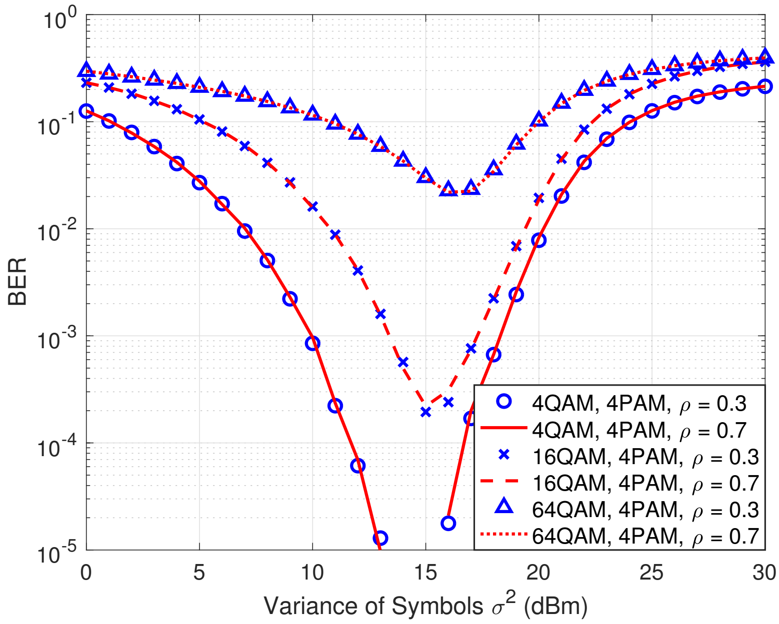

Figure 6. BER performance of the proposed DCHO-OFDM scheme under different variances of signal.

For a target BER of 2×10^{-3}, we further explore the spectrum efficiency of the proposed scheme, as depicted in Figures 7 and 8, in a scenario of high (−2 dBm) and of low (−8 dBm) noise power, respectively. For comparison, the spectrum efficiency of DCO-OFDM and the dimmable HACO-OFDM proposed in [22] are also provided. Upon observing, the achievable spectrum efficiency of DCHO-OFDM is superior to that of the conventional DCO-OFDM and HACO-OFDM in a wide range of dimming levels, where the transmission in DCO-OFDM is easily affected by dimming control due to the non-linear distortion. Furthermore, in contrast to HACO-OFDM scheme, while it has to detect ACO-OFDM signal first and then demodulatethe PAM-DMT signal, our proposed scheme can be detected upon utilizing the same receiver as the DCO-OFDM scheme, beneficially decreasing the complexity of receiver. Therefore, the proposed DCHO-OFDM scheme may be further cooperated with DCO-OFDM regime for a VLC system to satisfy the different transmission and illumination requirements, without increasing the complexity at the receiver side.

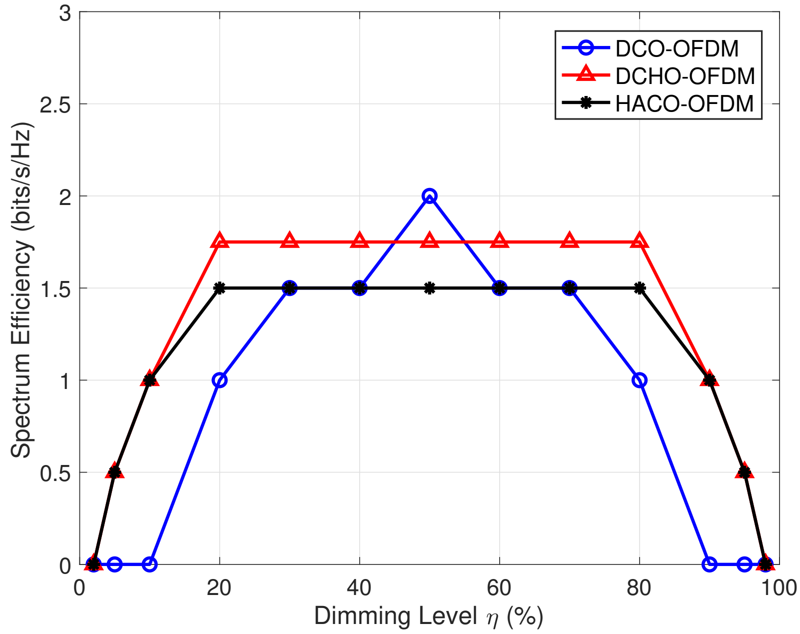

Figure 7. The achievable spectrum efficiency as a function of dimming level η, under a noise power of -2 dBm.

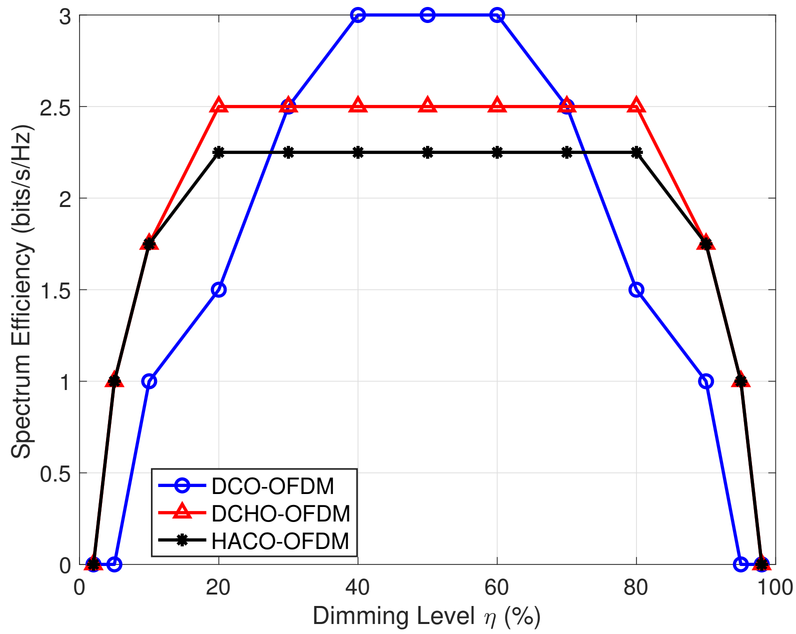

Figure 8. The achievable spectrum efficiency as a function of dimming level η, under a noise power of -8 dBm.

5. Conclusions

In this contribution, a novel DCHO-OFDM scheme was conceived for simultaneously achieving the dual functionality of data transmission and illumination in VLC. To achieve high spectrum efficiency, the bipolar unclipped ACO-OFDM signal was elaborately combined with the unipolar down-clipped PAM-DMT signal during the OFF state of PWM signal, while it was jointly transmitted with the upper-clipped PAM-DMT signal during the ON state. For the purpose of dimming control, a time-varying bias was applied to convert the superposed bipolar signals to unipolar ones, so that the PWM signal can be invoked without introducing interference. According to our simulations, a wide dimming range was obtained in DCHO-OFDM, with a high spectral efficiency and less fluctuation.

As the interference generated by the proposed scheme is orthogonal to the transmitted information, the demodulation of DCHO-OFDM can be easily executed upon employing a standard OFDM receiver, which may allow the proposed scheme to further cooperate with the DCO-OFDM scheme, fulfilling the dynamic communication and illumination requirements of the VLC system.

Author Contributions: Conceptualization, S.F.; Methodology, S.F.; Software, S.F.; Validation, H.F., Y.Z. and B.L.; Formal Analysis, S.F.; Investigation, H.F.; Resources, S.F.; Data Curation, S.F.; Writing–original Draft Preparation, S.F.; Writing–review & Editing, B.L.; Visualization, S.F.; Supervision, B.L.; Project Administration, H.F.; Funding Acquisition, B.L.

Funding: This research was supported in part by the National Natural Science Foundation of China under Grant 61571108, in part by the open research fund of National Mobile Communications Research Laboratory, Southeast University (No. 2019D18), in part by the Research Center of Optical Communications Engineering and Technology, Jiangsu Province (ZXF201902), and in part by the Fundamental Research Funds through the Central Universities under Grant JUSRP11919, in part by the Wuxi Science and Technology Development Fund (No. H20191001).

Conflicts of Interest: The authors declare no conflict of interest.

Appendix A

According to the definition of the upper-clipping, the upper-clipped PAM-DMT signal can be re-written as:

$$\lceil y_{PAM,n} \rceil_c = \frac{y_{PAM,n} - |y_{PAM,n}|}{2}. \tag{A1}$$

Upon taking the N-point FFT of signal $\lceil y_{PAM,n} \rceil_c$, we can get:

$$\begin{aligned} Y_k^c &= \sum_{n=0}^{N-1} \lceil y_{PAM,n} \rceil_c \exp\left(-j\frac{2\pi nk}{N}\right) \\ &= \underbrace{\frac{1}{2}\sum_{n=0}^{N-1} y_{PAM,n} \exp\left(-j\frac{2\pi nk}{N}\right)}_{W_1} - \underbrace{\frac{1}{2}\sum_{n=0}^{N-1} |y_{PAM,n}| \exp\left(-j\frac{2\pi nk}{N}\right)}_{W_2}. \end{aligned} \tag{A2}$$

It can be found that the first term W_1 in (A2) is the FFT results of the unclipped signal $y_{PAM,n}$, which is the original transmitted PAM-DMT symbols carried by the imaginary parts of the even-indexed subcarriers. The second term of W_2 is viewed as the interference, imposed by the upper-clipping operation. Recall the property of $y_{PAM,n} = y_{PAM,n+N/2} = -y_{PAM,N/2-n} = -y_{N-n}$ [14], the second term of (A2) can be re-written as:

$$\begin{aligned} W_2 = &\frac{1}{2}\sum_{n=1}^{N/4-1}\left[|y_{PAM,n}|\exp\left(-j\frac{2\pi nk}{N}\right) + |y_{PAM,N/2-n}|\exp\left(-j\frac{2\pi(N/2-n)k}{N}\right)\right. \\ &\left. +|y_{PAM,N/2+n}|\exp\left(-j\frac{2\pi(N/2+n)k}{N}\right) + |y_{PAM,N-n}|\exp\left(-j\frac{2\pi(N-n)k}{N}\right)\right] \\ = &\frac{1}{2}\sum_{n=1}^{N/4-1}|y_{PAM,n}|\left\{[1+\exp(-j\pi k)]\left[\exp\left(j\frac{2\pi nk}{N}\right) + \exp\left(-j\frac{2\pi nk}{N}\right)\right]\right\}. \end{aligned} \tag{A3}$$

Since we have

$$\exp(-j\pi k) = \begin{cases} -1, & k \text{ is odd-valued} \\ 1, & k \text{ is even-valued} \end{cases}, \tag{A4}$$

the second term W_2 can be further expressed as:

$$W_2 = \begin{cases} 0, & k \text{ is odd-valued} \\ \sum_{n=1}^{N/4-1} |y_{PAM,n}| \cos\frac{2\pi nk}{N}, & k \text{ is even-valued} \end{cases}. \tag{A5}$$

Upon observing, it can be easily found that the introduced interference caused by the upper-clipping falls only on the real parts of the even-indexed subcarriers, where the odd-indexed subcarriers and the imaginary parts of the even-indexed subcarriers are free of contamination. As a benefit, the proposed DCHO-OFDM scheme is capable of remaining uncorrupted by the upper-clipped PAM-DMT signal.

Appendix B

Upon taking the N-point FFT of z_n, we obtain the frequency-domain sample Z_K for $k = 0, 1, \cdots, N-1$ as:

$$\begin{aligned} Z_k &= \sum_{n=0}^{N-1} z_n \exp\left(-j\frac{2\pi nk}{N}\right) \\ &= z_0 + z_{\frac{N}{4}} \exp\left(-j\frac{\pi}{2}k\right) + z_{\frac{N}{2}} \exp\left(-j\pi k\right) + z_{\frac{3N}{4}} \exp\left(-j\frac{3\pi}{2}k\right) \\ &\quad + \sum_{n=1}^{N/4-1} \left[z_n \exp\left(-j\frac{2\pi nk}{N}\right) + z_{\frac{N}{2}-n} \exp\left(-j\frac{2\pi(\frac{N}{2}-n)k}{N}\right) \right. \\ &\qquad \left. + z_{\frac{N}{2}+n} \exp\left(-j\frac{2\pi(\frac{N}{2}+n)k}{N}\right) + z_{N-n} \exp\left(-j\frac{2\pi(N-n)k}{N}\right) \right]. \end{aligned} \tag{A6}$$

According to Proposition 1, we have $z_n = z_{N/2+n}$ for $n = 0, N/4$ and have $z_n = z_{N/2-n} = z_{N/2+n} = z_{N-n}$ for $n = 1, \cdots, N/4-1$. Therefore, the Equation (A6) can be re-written as:

$$\begin{aligned} Z_k &= \left[1 + \exp\left(-j\pi k\right)\right] \left[z_0 + z_{N/4} \exp\left(-j\frac{\pi}{2}k\right)\right] \\ &\quad + \sum_{n=1}^{N/4-1} z_n \left[1 + \exp\left(-j\pi k\right)\right] \left[\exp\left(-j\frac{2\pi nk}{N}\right) + \exp\left(j\frac{2\pi nk}{N}\right)\right]. \end{aligned} \tag{A7}$$

If the value of k is odd, where $\exp(-j\pi k) = -1$, then we have:

$$Z_k = 0, \quad k = 1, 3, 5, \cdots, N-1. \tag{A8}$$

Otherwise if the value of k is even, where $\exp(-j\pi k) = 1$, the expression of Z_k is therefore given by:

$$Z_k = 2z_0 + 2z_{N/4} \exp(-j\frac{\pi}{2}k) + 2\sum_{n=1}^{N/4-1} z_n \left[\exp\left(-j\frac{2\pi nk}{N}\right) + \exp\left(j\frac{2\pi nk}{N}\right)\right]. \tag{A9}$$

According to Euler formula, the real-part and the imaginary-part of Z_k are given by:

$$\mathfrak{Re}[Z_k] = 2z_0 + 2z_{N/4} \cos\frac{\pi k}{2} + 4\sum_{n=1}^{N/4-1} z_n \cos\frac{2\pi nk}{N}, \quad k = 0, 2, 4, \cdots, N-2, \tag{A10}$$

$$\mathfrak{Im}[Z_k] = 0, \qquad k = 0, 2, 4, \cdots, N-2. \tag{A11}$$

Upon observing Equations (A8), (A10) and (A11), it can be concluded that the interference generated by z_n is only imposed on the real part of the even-indexed subcarriers, leaving the odd-indexed subcarriers as well as the imaginary part of the even-indexed subcarriers uncontaminated.

References

1. Pathak, P.; Feng, X.; Hu, P.; Mohapatra, P. Visible light communication, networking and sensing: A survey, potential and challenges. *IEEE Commun. Surv. Tutor.* **2015**, *17*, 2047–2077. [CrossRef]
2. Bai, X.; Li, Q.; Tang, Y. A low-complexity resource allocation algorithm for indoor visible light communication ultra-dense networks. *Appl. Sci.* **2019**, *9*, 1391. [CrossRef]
3. Grobe, L.; Paraskevopoulos, A.; Hilt, J.; Schulz, D.; Lassak, F.; Hartlieb, F.; Kottke, C.; Jungnickel, V.; Langer, K. High-speed visible light communication systems. *IEEE Commun. Mag.* **2013**, *51*, 60–66. [CrossRef]
4. Rehman, S.; Ullah, S.; Chong, P.; Yongchareon, S.; Komosny, D. Visible light communications: A system perspective-Overview and challenges. *Sensors* **2019**, *19*, 1153. [CrossRef] [PubMed]
5. Feng, S.; Zhang, R.; Li, X.; Wang, Q.; Hanzo, L. Dynamic throughput maximization for the user-centric visible light downlink in the face of practical considerations. *IEEE Trans. Wirel. Commun.* **2018**, *17*, 5001–5015. [CrossRef]
6. Zuo, Y.; Zhang, J. A novel coding based dimming scheme with constant transmission efficiency in VLC systems. *Appl. Sci.* **2019**, *9*, 803. [CrossRef]
7. Feng, S.; Zhang, R.; Xu, W.; Hanzo, L. Multiple access design for ultra-dense VLC networks: Orthogonal vs non-orthogonal. *IEEE Trans. Commun.* **2019**, *67*, 2218–2232. [CrossRef]
8. Chen, Y.; Li, S.; Liu, H. Dynamic frequency reuse based on improved tabu search in multi-user visible light communication networks. *IEEE Access* **2019**, *7*, 35173–35183. [CrossRef]
9. Li, B.; Feng, S.; Xu, W.; Li, Z. Interference-free hybrid optical OFDM with low-complexity receiver for wireless optical communications. *IEEE Commun. Lett.* **2019**, *23*, 818–821. [CrossRef]
10. Chen, L.; Krongold, B.; Evans, J. Performance analysis for optical OFDM transmission in short-range IM/DD systems. *J. Lightw. Technol.* **2012**, *30*, 974–983. [CrossRef]
11. Dissanayake, S.; Armstrong, J. Comparison of ACO-OFDM, DCO-OFDM and ADO-OFDM in IM/DD systems. *J. Lightw. Technol.* **2013**, *31*, 1063–1072. [CrossRef]
12. Ranjha, B.; Kavehrad, M. Hybrid asymmetrically clipped OFDM-based IM/DD optical wireless system. *J. Opt. Commun. Netw.* **2014**, *6*, 387–396. [CrossRef]
13. Wang, Q.; Qian, C.; Guo, X.; Wang, Z.; Cunninghan, D.; White, L. Layered ACO-OFDM for intensity-modulated direct-detection optical wireless transmission. *Opt. Express* **2015**, *23*, 12382–12393. [CrossRef] [PubMed]
14. Wang, T.; Hou, Y.; Ma, M. A novel receiver design for HACO-OFDM by time-domain clipping noise elimination. *IEEE Commun. Lett.* **2018**, *22*, 1862–1865. [CrossRef]
15. Sun, Y.; Yang, F.; Gao, J. Comparison of hybrid optical modulation schemes for visible light communication. *IEEE Photon. J.* **2017**, *9*. [CrossRef]
16. Feng, S.; Bai, T.; Hanzo, L. Joint power allocation for the multi-user NOMA-downlink in a power-line-fed VLC network. *IEEE Trans. Veh. Technol.* **2019**, *68*, 5185–5190. [CrossRef]
17. Gancarz, J.; Elgala, H.; Little, T. Impact of lighting requirements on VLC systems. *IEEE Commun. Mag.* **2013**, *51*, 34–41. [CrossRef]
18. Wang, Z.; Zhong, W.; Yu, C.; Chen, J.; Francois, C.; Chen, W. Performance of dimming control scheme in visible light communication system. *Opt. Exp.* **2012**, *20*, 18861–18868. [CrossRef]
19. Wang, Q.; Wang, Z.; Dai, L. Asymmetrical hybrid optical OFDM for visible light communications with dimming control. *IEEE Photon. Technol. Lett.* **2015**, *27*, 974–977. [CrossRef]
20. Stevens, N.; Strycker, L.D. Single Edge Position Modulation as a Dimming Technique for Visible Light Communications. *J. Lightw. Technol.* **2016**, *34*, 5554–5560. [CrossRef]
21. Hany, E.; Little, T. Reverse polarity optical-OFDM (RPO-OFDM): Dimming compatible OFDM for gigabit VLC links. *Opt. Exp.* **2013**, *21*, 24288–24299.
22. Yang, F.; Gao, J. Dimming control scheme with high power and spectrum efficiency for visible light communications. *IEEE Photon. J.* **2017**, *9*. [CrossRef]
23. Li, B.; Xu, W.; Feng, S.; Li, Z. Spectral-efficient reconstructed LACO-OFDM transmission for dimming compatible visible light communications. *IEEE Photon. J.* **2019**, *11*. [CrossRef]
24. Lee, K.; Park, H. Modulations for visible light communications with dimming control. *IEEE Photon. Technol. Lett.* **2011**, *23*, 1136–1138. [CrossRef]
25. Armstrong, J.; Lowery, A. Power efficient optical OFDM. *Electron. Lett.* **2006**, *42*, 1. [CrossRef]

26. Li, B.; Xu, W.; Zhang, H.; Zhao, C.; Hanzo, L. PAPR reduction for hybrid ACO-OFDM aided IM/DD optical wireless vehicular communications. *IEEE Trans. Veh. Technol.* **2017**, *66*, 9561–9566. [CrossRef]
27. Lee, S.; Randel, S.; Breyer, F.; Koonen, A. PAM-DMT for intensity-modulated and direct-detection optical communication systems. *IEEE Photon. Technol. Lett.* **2009**, *21*, 1749–1751. [CrossRef]
28. Islim, M.; Haas, H. Augmenting the spectral efficiency of enhanced PAM-DMT-based optical wireless communications. *Opt. Express* **2016**, *24*, 11932–11949. [CrossRef] [PubMed]